Battery Evaluation Profiles for X-57 and Future Urban Electric Aircraft

Jeffrey C. Chin*,
Eliot D. Aretskin-Hariton †, Daniel J. Ingraham ‡,
Dustin L. Hall*, Sydney L. Schnulo*, Justin S. Gray*, Eric S. Hendricks*
NASA Glenn Research Center, Cleveland, OH, 44135

Battery energy density is one of the most critical design parameters for sizing all-electric aircraft, but it's easily overestimated. Establishing the effective, usable energy density is confused by varying degrees of margin needed to account for structural and thermal management between different cell chemistry and pack designs. A better methodology is needed to fairly compare emerging battery technologies for electric aircraft. Currently, there is a loss of critical information when vehicle trade studies are performed using "nominal" published cell-level performance metrics. Aircraft power demands rarely match these nominal power profiles, and aircraft designers lack the ability to accurately simulate the battery performance and temperature off-nominally unless the battery chemistry is well established. Conversely, battery suppliers are unable to publish more realistic performance metrics due to a lack of generalized reference cases. This can lead to poor assumptions. For example, aircraft studies may assume a fixed discharge efficiency of a battery, when in reality the usable energy in a pack is dependent on the power and thermal profile. Information needed to properly assess weight penalties for thermal management is also typically poorly characterized when assessing candidate batteries.

This paper serves to better inform battery development, and, similarly, provide aircraft designers with more realistic assumptions for applying knockdown margins in their designs. Detailed power and thermal performance estimates are described, which also provide a starting point for sizing power and thermal budgets using experimentally derived battery models. Results show that the average X-57 aircraft battery-to-shaft efficiency is 77.3% for a particular optimized mission. Considering a 25% reserve on the battery capacity, only close to half of the original 55.3kWh 'nominal' pack energy can be converted to useful work during a mission. Further estimates on a clean-sheet quad-rotor optimization show an average 82.7% battery-to-shaft efficiency, using 98% peak efficiency inverters and 97.4% peak efficiency motors. Although higher battery efficiencies are possible using larger packs, the resulting weight penalty negates improvement in vehicle performance. These trade-offs and resulting power profiles are provided as a starting point to better assess future battery designs.

I. Nomenclature

CAS	=	Calibrated Air Speed ($knots$)
C_D	=	drag coefficient
C_L	=	lift coefficient
ϵ	=	battery gravimetric energy density ($\frac{W*h}{kg}$)
η	=	efficiency
F_n	=	net thrust (N)
g	=	gravity ($\frac{m}{s^2}$)
I	=	current (A)
MTO	=	Mass at Take-Off (kg)
P	=	power (kW)
pax	=	# of passengers

*Propulsion Systems Analysis Branch, MS 5-11, AIAA Member
†Intelligent Control and Autonomy Branch
‡Acoustics Branch

R_{elec} = range (km)
R = internal cell resistance (Ω)
SOC = state-of-charge
T = temperature (K)
V = aircraft velocity $(\frac{km}{h})$
W = mass (kg)

II. Introduction

The energy sizing process for electric aircraft is fundamentally different than traditional fueled aircraft because battery efficiency varies with the size and temperature of the battery. This differs from traditional sizing problems, since fuel efficiency of an engine does not significantly vary with size or temperature of the fuel tank. This is further complicated by the more well known growth spiral factor challenge: changing the size of the "fuel tank" impacts the size and weight of other components, therefore changing the power demand. This creates a compounding cycle. Electric energy storage performance offers new degrees of freedom for engineers to optimize, but also makes comparison more challenging.

It's common for aircraft range to be estimated using high-level performance parameters using an equation known as the Breguet range equation. An electric equivalent to this equation has been established in previous papers [1] for vehicles in steady-level flight. Although this equation is helpful for understanding the connection between performance metrics, it's important to remember that unlike conventional gas turbine vehicles, the efficiency term is not constant, even for a fixed steady operating condition and fixed power setting. These range equations can be separately tailored for fixed-wing and Vertical Take-Off and Landing (VTOL) configurations, which are shown in Equations 1 and 2.

$$R_{elec,fixed} = \eta_{drive} \frac{3.6\epsilon}{g} \frac{C_L}{C_D} \frac{W_{batt}}{W_{TKO}} \tag{1}$$

$$R_{elec,VTOL} = \eta_{drive} \frac{F_n \epsilon}{g} \frac{V}{P} \frac{W_{batt}}{W_{TKO}} \tag{2}$$

In this equation, R is cruise range, η is the product of every drive-train component efficiency from the propeller to the battery, ϵ is the energy density of the battery, g is gravity, $\frac{C_L}{C_D}$ is the lift to drag ratio, and W represents battery and take-off mass. The 3.6 constant converts seconds to hours and meters to kilometers. The second equation includes velocity V, power P, and thrust F_n terms for vehicle bodies that don't produce lift. The conventional Breguet range equation compensates for the aircraft burning fuel/weight over the mission; however, the all-electric variant hides the effects of changing battery efficiency as the battery is depleted. The usefulness of this equation is also diminished by the fact that energy density is not an intrinsic pack property. Structural and thermal knockdowns must be applied to this metric to varying degrees depending on the specific mission configuration and current draw. The severity and sensitivity of these margins are explored in this paper.

Even for the well established chemistry such as the 18650 Li-ion cells chosen to fly on NASA's X-57 aircraft [2][3], the usable energy in a battery pack is challenging to calculate due to its non-linear dependence on the mission profile. The internal resistance in a battery is dependent on the state-of-charge and the temperature of the pack. During high power transients, the voltage of the pack drops, requiring even higher current draws on the system. This leads to a variable percentage of the stored energy being converted into waste heat, rather than doing useful work for the airplane. A battery capable of releasing 100kWh of energy slowly may only be able to release 90kWh for a more demanding discharge profile. Better accounting of cell internal resistance is important beyond quantifying how much energy can be converted to usable work. The resulting increase in heat must also be managed. Similar to other electrical components, we can treat this heat load as another sub-component efficiency:

$$\eta_{battery} = 1 - \frac{kW_{waste}}{kW_{tot}} = 1 - \frac{I^2 * R_{(SOC,T)}}{I * V_{(SOC,T,I)} + I^2 * R_{(SOC,T)}} \tag{3}$$

In equation 3: I, V, R, are the battery terminal current, voltage, and resistance, respectively. As denoted by the subscripts, terminal voltage is a function of current draw, and both voltage and resistance are functions of State-of-Charge

(SOC) and battery temperature (T). Emphasizing that they are not constant cannot be understated, yet these parameters are not well documented for many commercial batteries. These experimentally derived functions are documented in previous works [4] for the X-57 battery chemistry. This efficiency metric can be averaged over the whole mission to determine the overall percentage of the battery energy that was converted to heat versus work, however it is only valid for that specific battery chemistry and mission profile. As shown in Figure 2 the battery efficiency is reduced during high energy demands and will also drop off with diminished SOC as seen during the constant power segments. As a battery becomes less efficient, its temperature consequently changes, further impacting its efficiency. For the X-57 Li-ion chemistry, discharge efficiency is improved with increasing cell temperature, and is reduced at lower states of charge. This formulation is also constrained to a maximum temperature of 60°C, and minimum SOC of 20% to avoid accelerated performance degradation.

Equipped with a well characterized cell, battery, and vehicle model, optimization of the battery pack size can be performed as depicted in the following section using the X-57 vehicle as an example. This demonstrates the changing efficiency with pack size. In subsequent sections, a more generalized VTOL configuration is modeled. These clean sheet vehicle concepts additionally capture the "growth spiral" effects. In order to show these effects independently, the following section first conveys the battery efficiency dependence to the mission, and then the sensitivity to a different size or energy density battery is reviewed.

III. X-57 Efficiency Profile and Battery Case Weight Sensitivity

(a) X-57 Mod 4 Vehicle **(b) X-57 battery module**

Fig. 1 Isometric View of the Quadrotor Reference Vehicles

X-57, NASA's all electric experimental aircraft shown in Figure 1a, is chosen as the starting reference point, since the configuration has already advanced beyond the critical design stage. An image of a single battery module is also shown in Figure 1b. Although the mission for this experimental platform is not necessarily representative of future passenger vehicles, Table 1 shows the varying efficiency estimates as a baseline for various phases of flight.

Table 1 Average Efficiencies At Various Mission Segments

Phase	Batt. Power	Duration	Batt. η	Drive η*	Batt. to Shaft η
Taxi	34.0 kW	300s	97.0%	79.4%	77.0%
Motor Check	187.8 kW	30s	88.3%	89.1%	78.7%
Take-Off	189.3 kW	15s	87.6%	89.2%	78.1%
Climb	156.8 kW	446s	88.6%	88.8%	78.7%
Cruise	141.6 kW	417s	89.1%	88.4%	78.8%
Descent	31.4 kW	293s	95.1%	77.2%	73.4%
Total**	104.1 kW	1501s	91.7%	84.6%	77.3%

* Drive-train includes the wire, power electronics, and motors. It does not include the approx. 76% installed propeller efficiency

** Totals are duration averaged.

The table shows that the electric drive system, which consists of power cables, power electronics, and the motors, operates most efficiently during the climb and cruise phases. These values are based on design efficiency and do not include as-fabricated knockdowns. The motor and inverter efficiency models also do not include voltage-dependent efficiency impacts. The battery discharge efficiency is shown to be the lowest during the highest power segments. The solid line in Figure 2 shows the same individual phase segment table data plotted as a time history for the battery. The legend label "128/40" refers to the pack configuration of 128 series and 40 parallel battery strings. The different colors correspond to each flight segment. The extent to which these efficiencies could be improved, as depicted by the additional dashed lines, are discussed next.

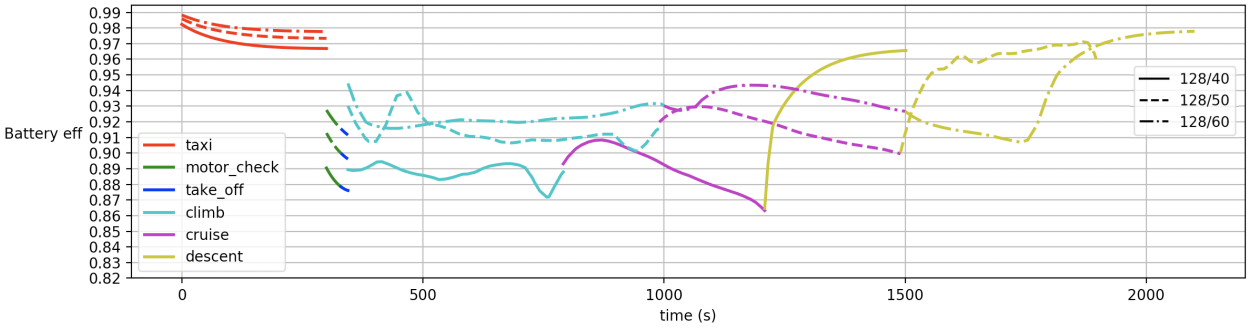

Fig. 2 Comparison of Battery Efficiency Histories over the Mission for Three Pack Sizes

Increasing the number of batteries in parallel directly divides the current required by each string, assuming a well-balanced pack and effective battery management system (BMS). A larger battery will not only result in a higher capacity, but also a more efficient battery. From this, it can be inferred that a 10% increase in battery size may lead to more than a 10% increase in useful work. The point at which the weight penalty overcomes this efficiency benefit will be vehicle-dependent. Although power-train efficiency is the dominant factor for range in long-range, fixed-wing vehicles, weight is typically the principle metric for VTOL vehicles.

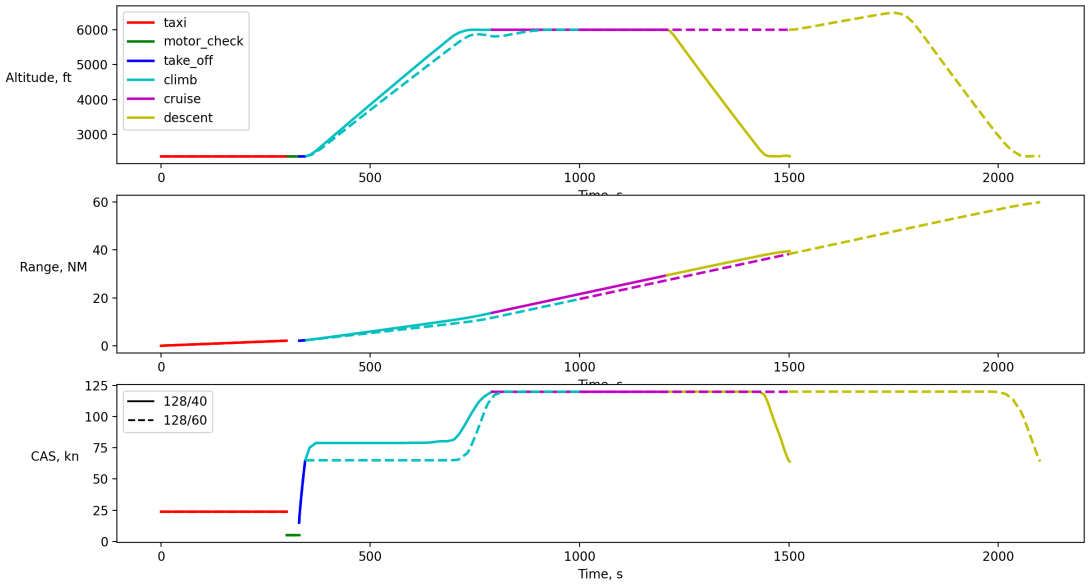

Fig. 3 Maximum Range Flight Profiles for Varying Battery Pack Sizes.

Both Figure 2 and the corresponding flight profiles in Figure 3 show the variation in battery efficiency for different cell configurations. All three analyzed pack configurations contain 128 cells connected in series, with curves shown for 40, 50, and 60 parallel strings. These corresponded to an average discharge efficiency of 91%, 93%, and 95%, respectively. Unsurprisingly, the vehicle with the largest battery discharged the most efficiently. The range of the vehicle was improved from 39 to 48 miles when battery capacity was increased by 25%. Range was increased to 60nm when battery capacity was increased by 50%, as shown in Figure 3. This increase in weight impacts the vehicle's ability to climb and doesn't consider other components such as the fuselage and landing gear, which may no longer be advantageously sized for the weight. Reducing the parallel string below 40 cells will have a much more adverse range and efficiency penalty. Even a small change from 40 to 38 parallel cells causes a 1% drop in efficiency, which can quickly lead to an infeasible design for both energy and thermal reasons.

Next, the impact of improving the X-57 energy density is explored while keeping the pack size fixed. The energy density is defined to include the full packaging weight of the battery modules. The individual cells on X-57 have a "nominal" energy density of 225 Wh/kg and the pack has a nominal energy density of 149 Wh/kg (55.3 kWh total, 370.86 kg total). Since approximately 125kg is dedicated to packaging, halving the packaging would bring the effective pack energy density to 180 Wh/kg.

Halving pack overhead results in a 23-second faster optimal climb and extends cruise by 31 seconds. Although the savings do not appear to be much, it does increase the maximum cruise segment range objective from 15.7 nm to 16.8 nm. Increasing the power density from 149 Wh/kg to 180 Wh/kg resulted in a 0.2% higher average battery efficiency and a 0.64% decrease in the averaged power requirement. These two benefits extend maximum range by 7.0%. These modest improvements are magnified in a clean-sheet vehicle design, as saved battery weight can cascade to further weight savings on the design of other components. This will be the focus of the remainder of the paper.

IV. VTOL Profile

Urban air mobility VTOL vehicles have few design precedents for battery manufacturers to follow. In the following section, usable energy density, payload, and range are swept as an input to the model, with required power profile as an output. Regressions on these swept variables can be used as a starting point for bench-marking and testing various battery metrics. Any necessary rejected heat power from the battery is also converted into a weight and efficiency penalty to be added to the input. This gives designers freedom to optimize energy density, discharge efficiency, thermal

performance, series/parallel configuration, and packing strategy freely without needing in-depth knowledge of the vehicle architecture. It also provides a definitive testing metric to accomplish a given mission. Additional real-world battery constraints on volume and cycle life are not included as design parameters but should be addressed in future work.

(a) 1 passenger **(b) 6 passenger**

Fig. 4 Isometric View of the Quadrotor Reference Vehicles

A battery powered quadrotor model was created as a reference vehicle, building on work from previous sizing efforts [5],[6]. This vehicle was sized for two different missions [7]. The first mission is a single passenger (250lb) payload and the second higher throughput variant is a six passenger (1200lb) payload. These particular missions are examined because they have the most advantageous or attainable characteristics for battery powered flight [8]. Results are shown for both missions swept across multiple ranges. For each design point, the vehicle size is re-optimized to minimize take-off mass and trajectories are optimized subjected to minimum altitude requirements in Table 2 using the flight profiles shown in Figure 5. The shape of these profiles are driven by battery temperature constraints and are discussed in greater detail in prior works [6]. To summarize, it's more weight optimal for the vehicle to climb to higher altitudes to keep the battery cool; rather than scaling up the size of the thermal system.

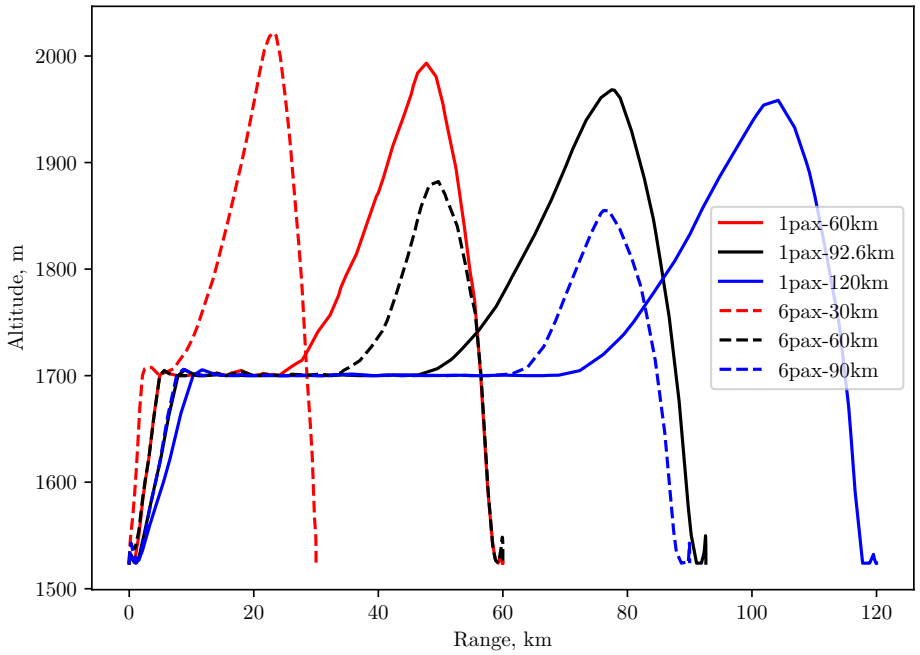

Fig. 5 400 Wh/kg Battery, Range Sweep, Minimized Vehicle Mass

Next, both missions are swept across varying energy densities in Table 3. Regressions on key parameters from this table are included in the appendix. As discussed previously, this installed energy density includes the entire pack weight and 20% SOC margin. For example, if a 3.53Ah, 3.4V cell that weighs 30 grams can only be discharged 80% and

Table 2 Design Optimization Results at Different Mission Ranges

Mission		**1pax, 250lb**			**6pax, 1200lb**		
System	**Parameter**	60km	92.6km	120km	30km	60km	90km
Vehicle	Takeoff Mass, kg	414.08	465.23	519.02	1034.55	1130.50	1254.84
Battery	Total Energy, kW*h	32.08	52.09	73.14	49.91	89.11	138.62
	Max Pack Discharge, A	97.68	117.96	139.81	239.17	262.45	303.65
	Energy Density, W*h/kg	400	400	400	400	400	400
	Mass, kg	64.12	104.10	146.17	99.75	178.09	277.04
	Avg Battery η	0.907	0.931	0.942	0.848	0.901	0.925
TMS	Max Power, kW	0.89	0.76	0.75	4.52	3.43	3.00
	Mass, kg	6.97	6.82	6.99	25.27	21.37	20.63
Propulsion	Shaft Power, kW	11.48	14.04	16.77	28.52	34.28	41.25
	Motor Mass, kg	3.52	4.03	4.58	6.93	8.08	9.47
Structures	Rotor Diameter, m	3.66	3.66	3.66	5.50	5.50	5.50
	Rotor Mass, kg	7.14	7.14	7.14	13.05	13.42	13.90
	Fuselage Mass, kg	51.02	55.32	59.70	96.44	102.58	110.30
	Landing Gear Mass, kg	37.76	40.89	44.06	70.72	75.18	80.78

requires an additional 28% of the cell weight at the pack level, it has a $(3.53 * 3.4 * 0.8)/(0.03 * 1.28) = 250\frac{Wh}{kg}$ installed usable energy density. The "nominal" spec sheet for this battery may be advertised as $(3.53 * 3.4)/(0.03) = 400\frac{Wh}{kg}$. As seen on X-57 and in the following sections, additional energy will be lost to heat due to the demanded current draw.

The battery discharge profile steadily rises in current as the battery voltage drops. Power demand stays roughly constant throughout climb and cruise, with a brief drop for descent before a full power landing. The optimal trajectory understandably operates motors at their peak optimal efficiency for as long as possible. A more constrained mission with additional hover, climb, or altitude constraints would likely come off this boundary more frequently, at the cost of a heavier design.

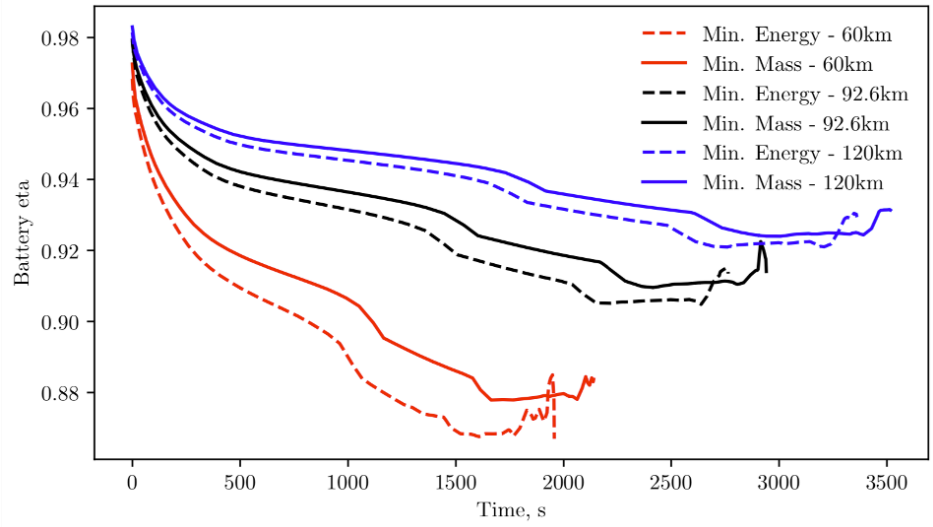

Fig. 6 Battery Efficiency Profile Swept Across Multiple Ranges, 1 Passenger

As the SOC of the battery decreases, the voltage of the battery decreases, resulting in a higher cell current draw. Internal resistance in the cell also increases with diminished capacity, which combine to result in a drop in efficiency over the course of the mission. This causes the battery to drain more quickly near the end of the flight, as well as

Table 3 Design Optimization Results at Different Energy Densities.

Vehicle Size		**1pax, 250lb**				**6pax, 1200lb**			
System	**Parameter**	250Wh/kg	300Wh/kg	350Wh/kg	400Wh/kg	250Wh/kg	300Wh/kg	350Wh/kg	400Wh/kg
Vehicle	Takeoff Mass, kg	618	538	494	465	1380	1277	1174	1130
	Range, km	92.6	92.6	92.6	92.6	60.0	60.0	60.0	60.0
Battery	Total Energy, kW*h	69.17	60.05	55.28	52.09	106.83	98.86	92.44	89.11
	Max Pack Discharge, A	179.52	146.77	129.38	117.96	348.73	316.84	277.85	262.45
	Energy Density, W*h/kg	250	300	350	400	250	300	350	400
	Mass, kg	221.36	160.13	126.32	104.10	341.88	263.61	211.24	178.09
	Avg Batt η	0.921	0.926	0.929	0.931	0.892	0.897	0.899	0.901
TMS	Max Power, kW	1.14	0.92	0.90	0.76	4.26	3.79	3.51	3.43
	Mass, kg	9.47	8.05	7.16	6.82	28.15	24.50	22.45	21.37
Propulsion	Shaft Power, kW	21.63	17.60	15.43	14.04	45.40	40.11	36.67	34.28
	Motor Mass, kg	5.55	4.74	4.31	4.03	10.30	9.24	8.55	8.08
Structures	Rotor Diameter, m	3.66	3.66	3.66	3.66	5.50	5.50	5.50	5.50
	Rotor Mass, kg	7.41	7.14	7.14	7.14	20.58	20.05	13.62	13.42
	Fuselage Mass, kg	67.40	61.19	57.67	55.32	117.84	111.64	105.32	102.58
	Landing Gear Mass, kg	49.66	45.15	42.59	40.89	86.26	81.75	77.16	75.18

generate more heat. Figure 6 and 7 show the importance of sizing both the battery and thermal management system to handle the battery performance at the end of the mission. Figure 6 also shows an interesting trend in the optimal battery size for short range vehicles. The 60km case shows a dramatic reduction in elected battery efficiency, indicating the optimizer chose to under-size the battery relative to the other missions. This means weight becomes more critical to the optimal mission as the design range decreases. A key note is that the battery temperature starts at 35C and is limited to 50C on all of these designs. Consequently, the shorter range case can afford to expend more heat at a faster rate, given the shorter flight duration. Follow-on work will look at maintaining a smaller delta between starting and ending temperature to more realistically simulate back-to-back missions. Another non-intuitive trend is the relatively lower battery efficiency for the minimum energy vehicle. These vehicles sacrificed battery efficiency for higher drive-train efficiency by using heavier heat exchangers. Larger heat exchangers require less energy to keep the batteries cool. Less energy was also a consequence of the optimal trajectory for the minimum energy vehicles being slightly shorter in duration for all cases. Figure 7 sweeps energy density, showing very minimal impacts to the optimal vehicle proportions. Instead, the entire vehicle is scaled as shown in Table 3. Additional variables for each of these design sweeps are included in Figure 10a in the appendix.

Figure 8 shows an interesting trend in optimized drive-train efficiency when comparing the minimum energy optimum and minimized weight optimum. The disparity between the two is largest when the achievable energy density is the highest. Intuitively, the highest efficiency is expected to always be the optimal case; however, this leads to a heavier vehicle weight. The drop in efficiency for the mass optimized vehicles is a result of increased thermal management system power draw. The wattage consumed by the coolant loop is considered an efficiency loss on the drive-train, and the lighter vehicle saves substantial weight on the battery at the cost of requiring higher power cooling. Additional profiles are included in the appendix for the six-passenger vehicle variant.

V. Conclusions and Future Work

This paper examined mission-dependent battery waste heat starting with a notional X-57 mission. Performance impacts from battery size and energy density were quantified for a statically sized, fixed-wing vehicle. Next, a VTOL quadrotor was optimally sized for various ranges and achievable energy density. The variation in sensitivity between each of these missions highlights the need for openly available surrogate models to give battery system engineers more realistic benchmarks for designing batteries. Additional real-world constraints like volume and degradation are not evaluated explicitly but can be posed as additional weight penalty margins, if they exceed certain thresholds.

This paper shows the energy and thermal sizing impacts for a specific Li-ion battery chemistry. Future work will

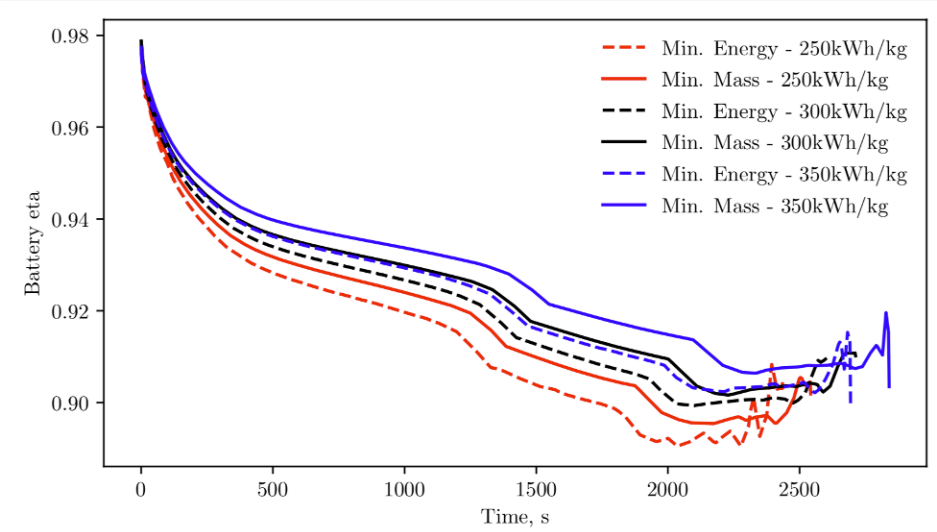

Fig. 7 Battery Efficiency Profile Swept Across Multiple Energy Densities, 1 Passenger

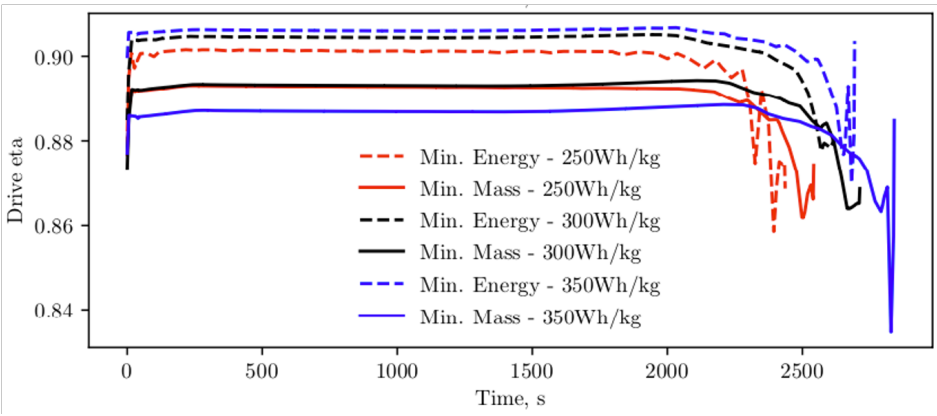

Fig. 8 Drive-train Efficiency Profile over Optimized Trajectories Across Multiple Energy Densities

attempt to create chemistry agnostic sensitivity functions with weight and thermal loads as the input and power profiles as the output. Follow-on studies are currently being conducted to better determine pack weight knockdowns based on the magnitude of the waste heat and the size of the thermal system. As new electric VTOL configurations are developed, understanding realistic energy density and efficiency values will be critical for creating optimally sized vehicles. Ideally, these results help assist in scoping the magnitude of the battery design challenge and can be used to help set productive benchmarks.

Appendix

Regressions on each swept design variable are provided in the following section: Energy Density is fixed as 400 Wh/kg for range cases. For the energy density cases, range is fixed at 92.6km for the 1 passenger vehicle, and 60km for the 6 passenger vehicle.

Table 4 Regressions for Various Parameters Based on Range and Energy Density

Output (y)	Input (x)	1pax, 250lb	6pax, 1200lb
MTO (kg)	Range (km)	$y = 0.0066x^2 + 0.5666x + 356.43$	$y = 0.0158x^2 + 1.7788x + 966.99$
	$\epsilon(\frac{Wh}{kg})$	$y = 0.0052x^2 - 4.3553x + 1383.6$	$y = 0.0118x^2 - 9.7241x + 3131.8$
Pack Size (kWh)	Range (km)	$y = 0.0026x^2 + 0.221x + 9.5533$	$y = 0.0057x^2 + 0.7912x + 21.02$
	$\epsilon(\frac{Wh}{kg})$	$y = 0.0006x^2 - 0.4975x + 156.34$	$y = 0.0038x^2 - 3.546x + 981.45$
Max Discharge (A)	Range (km)	$y = 0.0029x^2 + 0.1761x + 76.593$	$y = 0.01x^2 - 0.12x + 233.81$
	$\epsilon(\frac{Wh}{kg})$	$y = 0.0021x^2 - 1.7906x + 493.39$	$y = 0.0047x^2 - 3.8465x + 1046.2$
Avg Battery Eff (%)	Range (km)	$y = -0.0006x^2 + 0.1654x + 82.879$	$y = -0.0017x^2 + 0.3292x + 76.385$
	$\epsilon(\frac{Wh}{kg})$	$y = -2E^{-5}x^2 + 0.0226x + 87.954$	$y = 0x^2 + 0.004x + 88.5$

Further variable trends for the 6 passenger variant are included below.

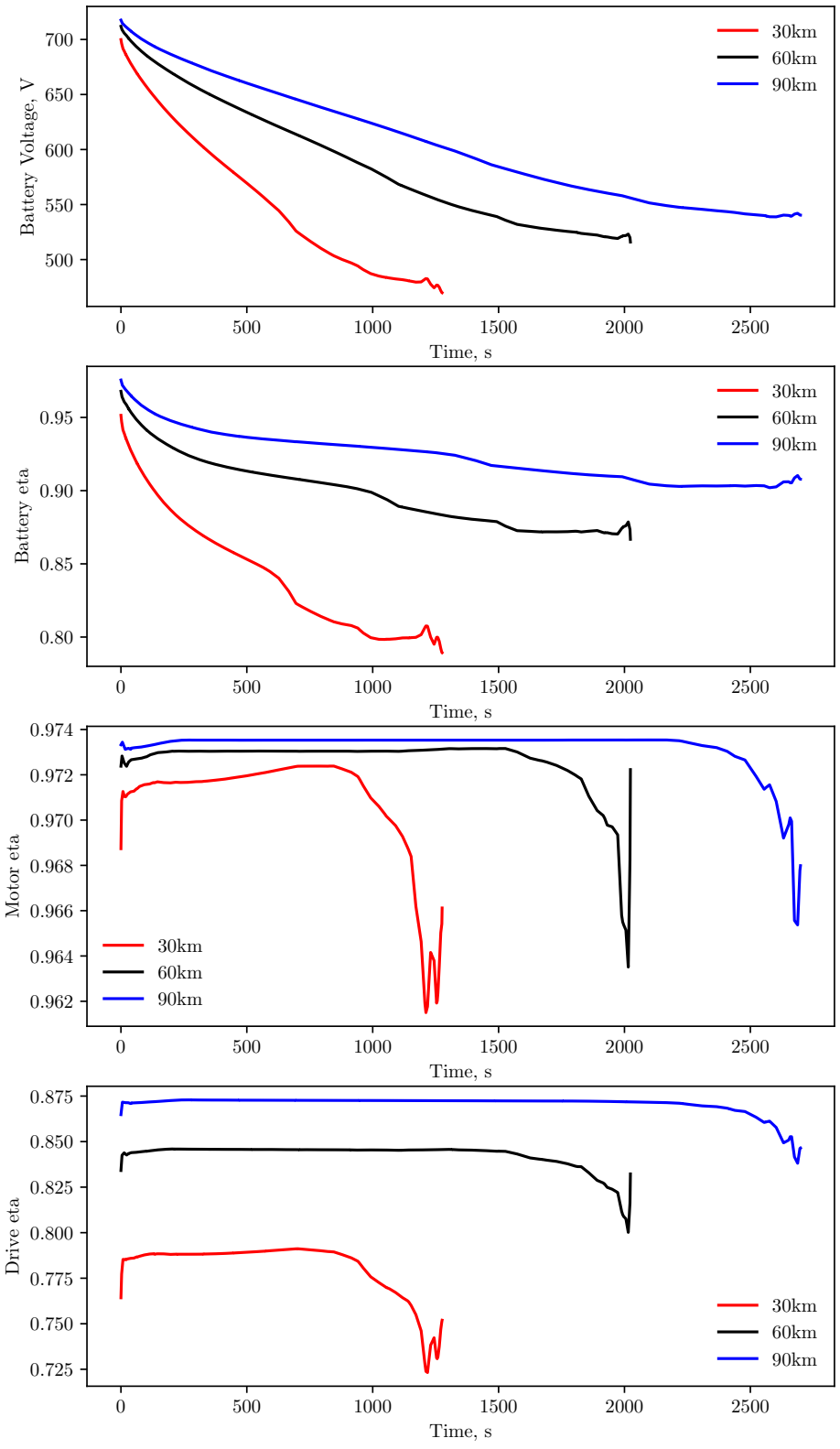

Fig. 9 400 Wh/kg Battery, Range Sweep, Minimum MTO, 6 Passenger

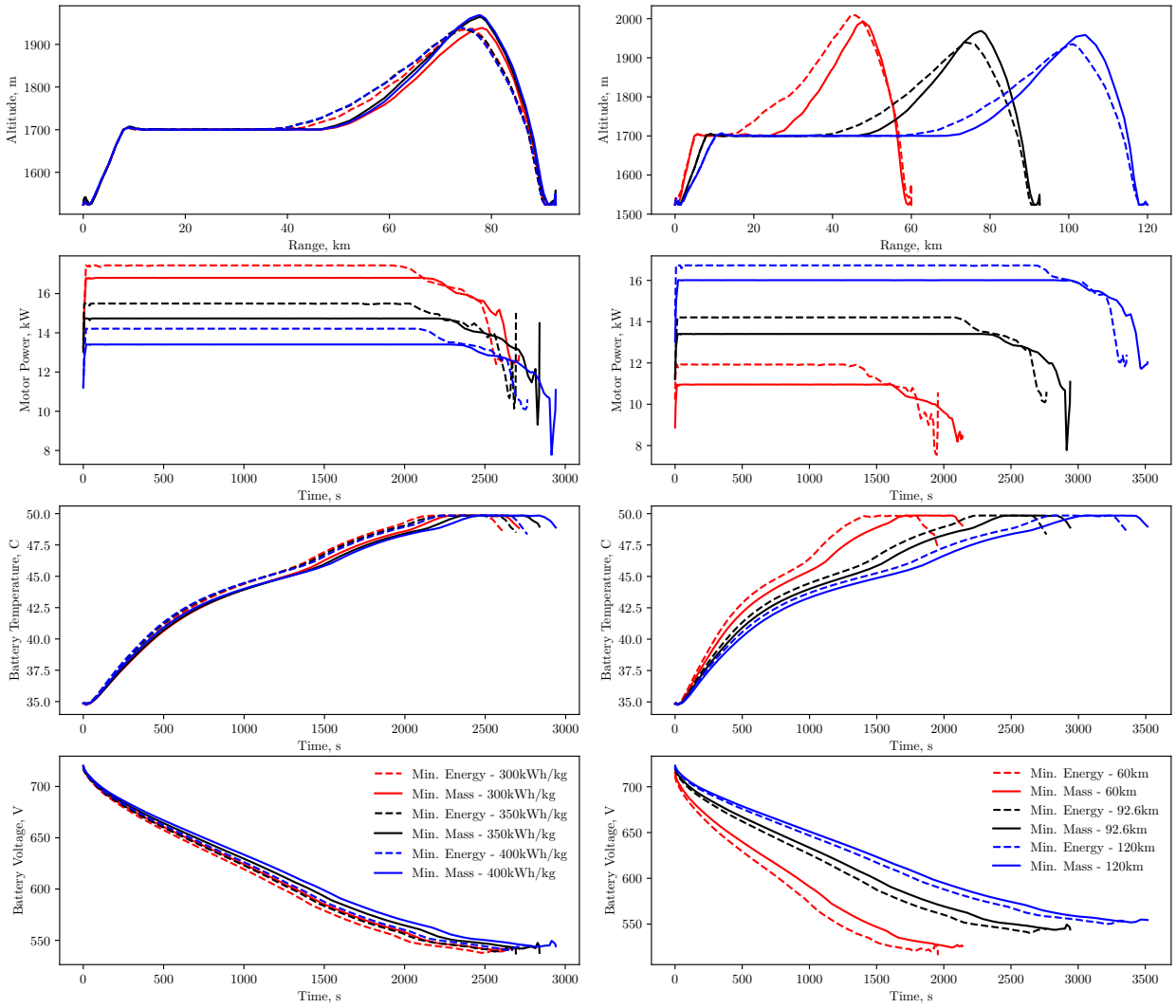

(a) Battery Sweep **(b) Range Sweep**

Fig. 10 Additional Parameters, 1 Passenger Variant

Acknowledgments

The authors would like to thank the the X-57 team and the Aviary team for providing the engineering design and modeling starting point for this work. Additional thanks to the NASA Transformational Technologies and Toolsets (TTT) and Flight Demonstration and Capabilities (FDC) projects for each sponsoring aspects of this work.

References

[1] Hepperle, M., "Electric Flight – Potential and Limitations," *German Aerospace Center*, NATO, mMH-Aerotools, 2012. URL `https://www.mh-aerotools.de/company/paper_14/MP-AVT-209-09.pdf`.

[2] Johnson, W., Silva, C., and Solis, E., "X-57 Power and Command System Design," *IEEE Explore*, 2017 IEEE Transportation Electrification Conference and Expo (ITEC), IEEE, 2017. https://doi.org/10.1109/ITEC.2017.7993303, URL https://ntrs.nasa.gov/archive/nasa/casi.ntrs.nasa.gov/20170005797.pdf.

[3] Borer, N. K., Patterson, M. D., Viken, J. K., Moore, M. D., Bevirt, J., Stoll, A. M., and Gibson, A. R., "Design and Performance of the NASA SCEPTOR Distributed Electric Propulsion Flight Demonstrator," *16th AIAA Aviation Technology,*

Integration, and Operations Conference, AIAA Aviation, American Institute of Aeronautics and Astronautics, 2016. https://doi.org/doi:10.2514/6.2016-3920, URL http://dx.doi.org/10.2514/6.2016-3920.

[4] Chin, J. C., Schnulo, S. L., Miller, T. B., Prokopius, K., and Gray, J., "Battery Performance Modeling on Maxwell X-57," *AIAA Scitech 2019 Forum*, AIAA Aviation, American Institute of Aeronautics and Astronautics, 2019. https://doi.org/doi:10.2514/6.2016-3920, URL https://arc.aiaa.org/doi/pdf/10.2514/6.2019-0784.

[5] Johnson, W., Silva, C., and Solis, E., "Concept Vehicles for VTOL Air Taxi Operations," *AIAA Aviation 2019 Forum*, AHS Specialists Conference on Aeromechanics Design for Transformative Vertical Flight, American Helicopter Society, 2018. https://doi.org/doi:20180003381, URL https://ntrs.nasa.gov/search.jsp?R=20180003381.

[6] Hendricks, E. S., Aretskin-Hariton, E. D., Ingraham, D. J., Gray, J. S., Schnulo, S. L., Chin, J. C., Falck, R. D., and Hall, D. L., "Multidisciplinary Optimization of a Turboelectric Tiltwing Urban Air Mobility Aircraft," *AIAA Aviation 2020 Forum*, AIAA Aviation, American Institute of Aeronautics and Astronautics, 2020. https://doi.org/doi:10.2514/6.2019-3551, URL https://arc.aiaa.org/doi/pdf/10.2514/6.2019-3551.

[7] Patterson, M. D., Antcliff, K. R., and Kohlman, L. W., "A Proposed Approach to Studying Urban Air Mobility Missions Including an Initial Exploration of Mission Requirements," NASA Tech Report Server, 2019. URL https://ntrs.nasa.gov/archive/nasa/casi.ntrs.nasa.gov/20190000991.pdf.

[8] Silva, C., Johnson, W., Patterson, M. D., and Antcliff, K. R., "VTOL Urban Air Mobility Concept Vehicles for Technology Development," NASA Tech Report Server, 2019. URL https://rotorcraft.arc.nasa.gov/Publications/files/vtol-urban-air-2.pdf.